SOLID-STATE PHYSICS

Spin-selective tunneling from nanowires of the candidate topological Kondo insulator SmB_6

Anuva Aishwarya[1], Zhuozhen Cai[1], Arjun Raghavan[1], Marisa Romanelli[1], Xiaoyu Wang[2], Xu Li[3], G. D. Gu[4], Mark Hirsbrunner[1], Taylor Hughes[1], Fei Liu[3]*, Lin Jiao[1,2]*, Vidya Madhavan[1]*

Incorporating relativistic physics into quantum tunneling can lead to exotic behavior such as perfect transmission through Klein tunneling. Here, we probed the tunneling properties of spin-momentum-locked relativistic fermions by designing and implementing a tunneling geometry that uses nanowires of the topological Kondo insulator candidate samarium hexaboride. The nanowires are attached to the end of scanning tunneling microscope tips and used to image the bicollinear stripe spin order in the antiferromagnet $Fe_{1.03}Te$ with a Neel temperature of about 50 kelvin. The antiferromagnetic stripes become invisible above 10 kelvin concomitant with the suppression of the topological surface states in the tip. We further demonstrate that the direction of spin polarization is tied to the tunneling direction. Our technique establishes samarium hexaboride nanowires as ideal conduits for spin-polarized currents.

A direct consequence of the nontrivial topology of Z_2 topological insulators (TIs) is the existence of an odd number of spin-momentum-locked boundary modes with Dirac dispersion (*1*). When the Fermi energy is tuned inside the bulk band gap, transport is dominated by the Dirac surface states, and marked topological phenomena can be observed. In this scenario, spin-momentum locking coupled with Dirac dispersion dictates that the net current traveling in a given direction must be spin polarized; currents traveling in opposite directions carry opposite spin. The high spin-charge conversion efficiency, and the topological protection of the boundary states, make TIs particularly interesting for applications in "topological spintronics," as well as for quantum technologies such as controlling qubits (*2*–*4*). To date, many exotic phenomena have been realized in magnetically doped TIs or TI heterostructures, such as the quantum anomalous Hall effect (*5*), the topological magnetoelectric effect (*6*), and the large spin–orbit torque effect (*7*). TI boundary modes are also ideal platforms with which to explore the unique tunneling properties of relativistic fermions.

In practice, a substantial bottleneck to using TIs both for fundamental studies and applications is the fact that many semiconductor-based TIs suffer from intrinsic defects that cause self-doping, which moves the Fermi energy into the bulk bands. There has therefore been a tremendous impetus to study interaction-driven topological phases in which the Fermi level is naturally pinned to the topological band gap. To this end, topological Kondo insulators (TKIs) have been proposed as ideal topological systems in which surface Dirac fermions naturally dominate the density of states near Fermi level (*8*). In TKIs, the lattice Kondo effect leads to the emergence of a low-energy, correlation-driven heavy band, which hybridizes with another light band crossing the Fermi energy, leading to a Kondo hybridization gap (*9*). A concomitant band inversion results in the formation of topological surface states (TSS) within this gap. The material samarium hexaboride (SmB_6) (Fig. 1A) has been proposed as a TKI and exhibits the following phenomenology (*9*). At high temperatures, SmB_6 is a Kondo metal. Below the bulk Kondo coherence temperature (T_K) of ~50 K, the hybridization between the emergent heavy f band and the light d bands opens a Kondo gap (Fig. 1B, schematic), which becomes better defined with decreasing temperature (*10*–*14*). Scanning tunneling microscopy (STM) studies have shown that, below 10 to 15 K, "heavy" surface states develop within the Kondo gap (*15*, *16*). The observation of the surface states at far lower temperatures (~10 K) than T_K suggests that the surface Kondo temperature may be lower than T_K (*15*, *17*). The topological nature of the surface states is supported by the observation of a series of phenomena (*18*), e.g., nonlocal transport (*19*, *20*), enhanced spin pumping (*21*), the Edelstein effect (*22*, *23*), chiral edge modes (*24*), spin-momentum locked spin textures for the surface states (*25*), and the Klein paradox (*26*). Despite these studies, the topological origin of the surface states remains controversial (*27*). If the surface states were indeed topological, then the presence of isolated TSS within a bulk band gap that straddles the Fermi energy would make SmB_6 an excellent system for harnessing the properties of Dirac electrons.

In this work, we used a unique tunneling geometry to reveal a distinctive tunneling process that we call helical tunneling. The term "helical" refers to a direction-dependent spin polarization akin to the spin-momentum locking of helical edge states of a quantum spin Hall insulator. We show that the tunneling electrons from SmB_6 nanowires are spin polarized, with the direction of spin polarization being tied to the direction of tunneling. To achieve this, we used focused ion beam–based nanofabrication techniques to harvest and attach SmB_6 nanowires to the ends of etched tungsten wires typically used as STM tips (see fig. S1) (*28*). The nanowires used in this work were grown on silicon (Si) substrates. They have diameters ranging from 60 to 100 nm and average lengths of ~50 μm (Fig. 1C, inset, and D). The growth procedure is described in detail elsewhere (*29*). The nanowires grow along the [001] direction and terminate laterally at high-symmetry facets such as (001). The larger-diameter nanowires that we used typically contain multiple large facets in which the electronic structure is expected to be similar to the surfaces of bulk SmB_6. Given that the penetration depth of TSS in SmB_6 is <30 nm, our SmB_6 nanowires are sufficiently thick to host TSS (*21*, *26*).

Mounting SmB_6 nanowires on tungsten tips is a two-step process that uses the omniprobe inside the focused ion beam + scanning electron microscopy (SEM) dual-beam system (*28*). The nanowire tips thus prepared are transferred to the STM (Fig. 1E shows a schematic of the tunneling setup). For benchmarking, we first characterized the tips on a Cu(111) single-crystal sample (see figs. S2 and S3) (*28*). Using the facts that the STM dI/dV spectrum is a convolution of tip and sample density of states and that Cu(111) has a flat density of states near the Fermi energy, we could isolate the density of states of the nanowire tip. The data verify that the nanowire tip hosts surface states similar to bulk SmB_6.

On the basis of these observations, we expect the surface states to play a key role in the tunneling characteristics of the nanowire tips. In particular, the spin-momentum locking of topological surface states may result in spin-polarized currents. To determine the spin polarization of the tunnel current, we studied iron telluride ($Fe_{1+x}Te$), which is a bicollinear antiferromagnet (AFM) for $x < 0.11$ (Fig. 2A). $Fe_{1+x}Te$ has been extensively studied by spin-polarized STM, and it is well established that the atomic-scale AFM order can be observed with a traditional magnetic tip, where it presents itself as stripes with double the tellurium (Te) periodicity (*30*–*32*) (Fig. 2, B and C). Because of the matrix element effects, tunneling is favored between

---

[1]Department of Physics and Materials Research Laboratory, University of Illinois Urbana-Champaign, Urbana, IL 61801, USA. [2]National High Magnetic Field Laboratory, Florida State University, Tallahassee, FL 32310, USA. [3]State Key Laboratory of Optoelectronic Materials and Technologies, Guangdong Province Key Laboratory of Display Material and Technology, and School of Electronics and Information Technology, Sun Yat-sen University, Guangzhou 510275, China. [4]Condensed Matter Physics and Materials Science Department, Brookhaven National Laboratory, Upton, NY 11973, USA.

***Corresponding author. Email: liufei@mail.sysu.edu.cn (F.L.); lin.jiao@magnet.fsu.edu (L.J.); vm1@illinois.edu (V.M.)**

spin parallel states and suppressed between spin antiparallel states (*33*).

For our STM studies, $Fe_{1+x}Te$ (nominal x = 0.03) single crystals were cleaved at ~90 K before inserting them into the STM head. Shown in Fig. 2H is an average dI/dV spectrum obtained on $Fe_{1+x}Te$ at 1.7 K. With SmB_6 on the tip, we observed a peak on the opposite side of E_F compared with spectra on bulk SmB_6 (see comparison with bulk spectrum in fig. S4) (*28*). This demonstrates the existence of the surface states on the tip. We then used this tip to obtain topographic images of $Fe_{1+x}Te$. In contrast to topography using a tungsten (W) tip (Fig. 2D), which shows the expected square Te lattice of the top layer with a lattice constant of 3.8 Å, the images with the SmB_6 nanowire tips show stripes (Fig. 2E). The double periodicity of the observed pattern is the same as the spin modulation of the striped AFM order (Fig. 2G), and the image is consistent with the spin-dependent contrast seen in several previous STM studies using magnetic tips (*30*–*32*). This phenomenology was confirmed

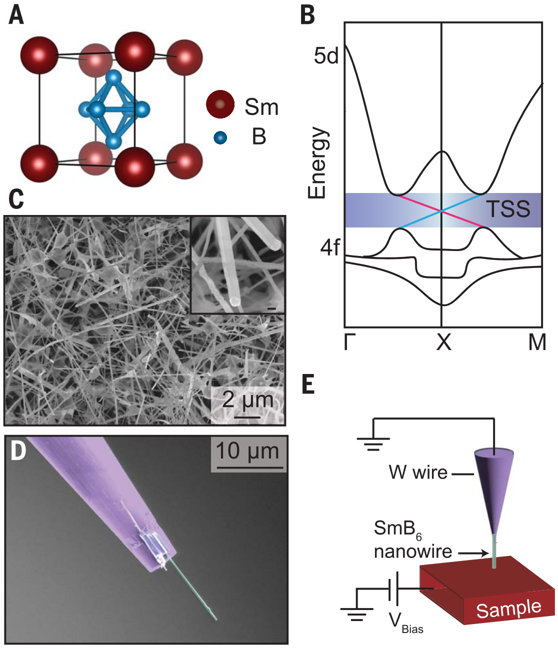

Fig. 1. Morphology, crystal structure, and electronic structure of the SmB_6 nanowire tip. (**A**) Crystal structure of SmB_6 showing the cubic lattice of Sm atoms with octahedrons of boron at the center. (**B**) Schematic of the band structure of SmB_6 showing the hybridization-induced gap between the 5d and 4f bands. The blue shaded region represents the Kondo gap, and the cyan and pink lines indicate the TSS. The colors represent opposite spin orientations. (**C**) High-resolution SEM image of the nanowires on a silicon substrate. Inset: magnified image of a nanowire. Scale bar, 200 nm. (**D**) High-resolution false-colored SEM image of the nanowire tip showing the nanowire bonded to a trimmed W tip. (**E**) Schematic of the STM circuit showing the nanowire tip and the sample.

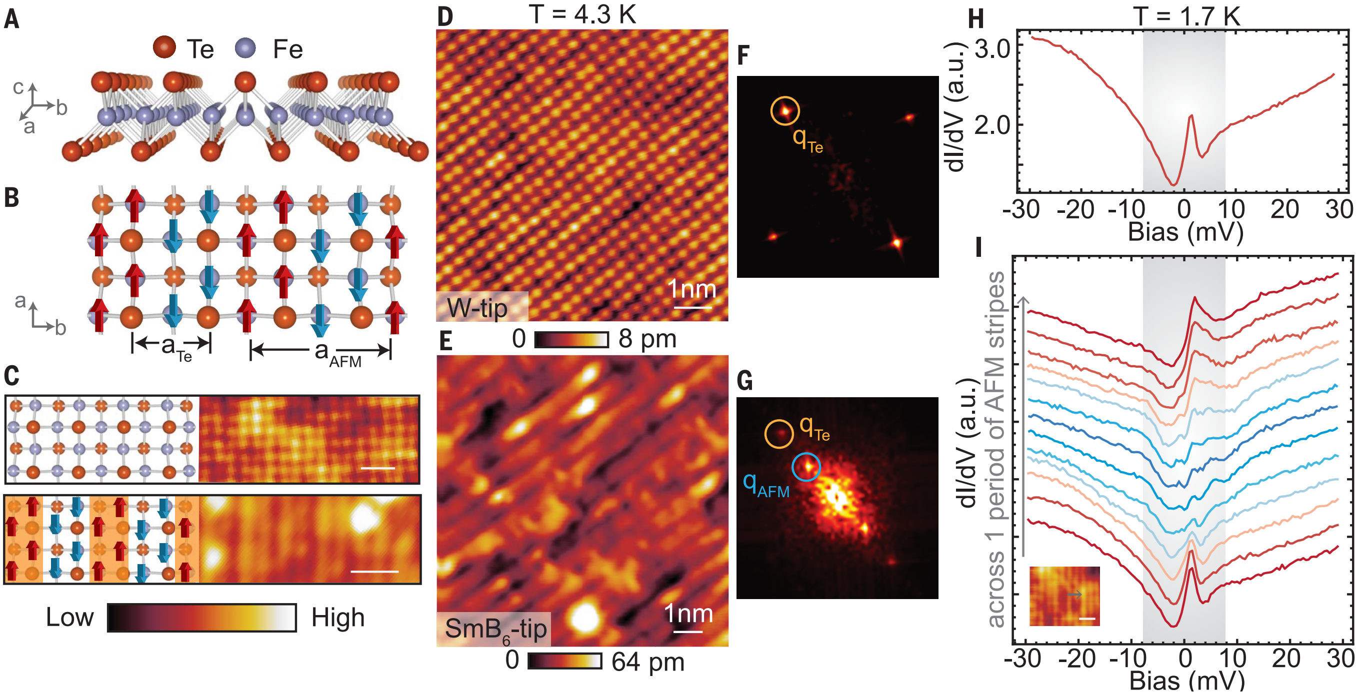

Fig. 2. Atomic-resolution imaging of antiferromagnetic stripes in $Fe_{1+x}Te$ with SmB_6 nanowire tip. (**A**) Crystal structure showing one layer of $Fe_{1+x}Te$ made of an iron (Fe) layer sandwiched between two Te layers. (**B**) Schematic of the *ab* plane of the lattice with the overlay of the spin structure showing the in-plane antiferromagnetic order. The periodicity of the antiferromagnetic order and the lattice are labeled as a_{AFM} and a_{Te}, respectively. (**C**) Schematic of the Te lattice is depicted by the orange spheres (top) and AFM order (bottom). Topography obtained with a W tip (top) and a spin-polarized Cr tip (bottom). The schematic and topography are not the same size. Scale bar in each topography, 1 nm. (**D**) STM topography obtained with a spin-averaging W tip (V_{Bias} = 20 mV, I = 60 pA, T = 4.3 K). (**E**) STM topography obtained with the SmB_6 tip at V_{Bias} = 20 mV, I = 60 pA, T = 4.3 K showing well-defined spin contrast. (**F** and **G**) FFT of the topographies in (D) and (E), respectively, showing only the Bragg peaks from the Te lattice (q_{Te}) in (F) and the presence of a strong signal from the antiferromagnetic ordering (q_{AFM}) along with the q_{Te} in (G). (**H**) Average dI/dV spectroscopy obtained on $Fe_{1+x}Te$ at T = 1.7 K (V_{Bias} = 50 mV, I = 120 pA). In (H) and (I), the highlighted gray region shows the feature in the DOS associated with the topological surface state. (**I**) dI/dV line cut across one period of the AFM stripe (red to blue to red) showing the modulation of the TSS peak as a function of position. Inset shows the topography and the gray arrow shows the line where the spectra were obtained. Scale bar, 1 nm.

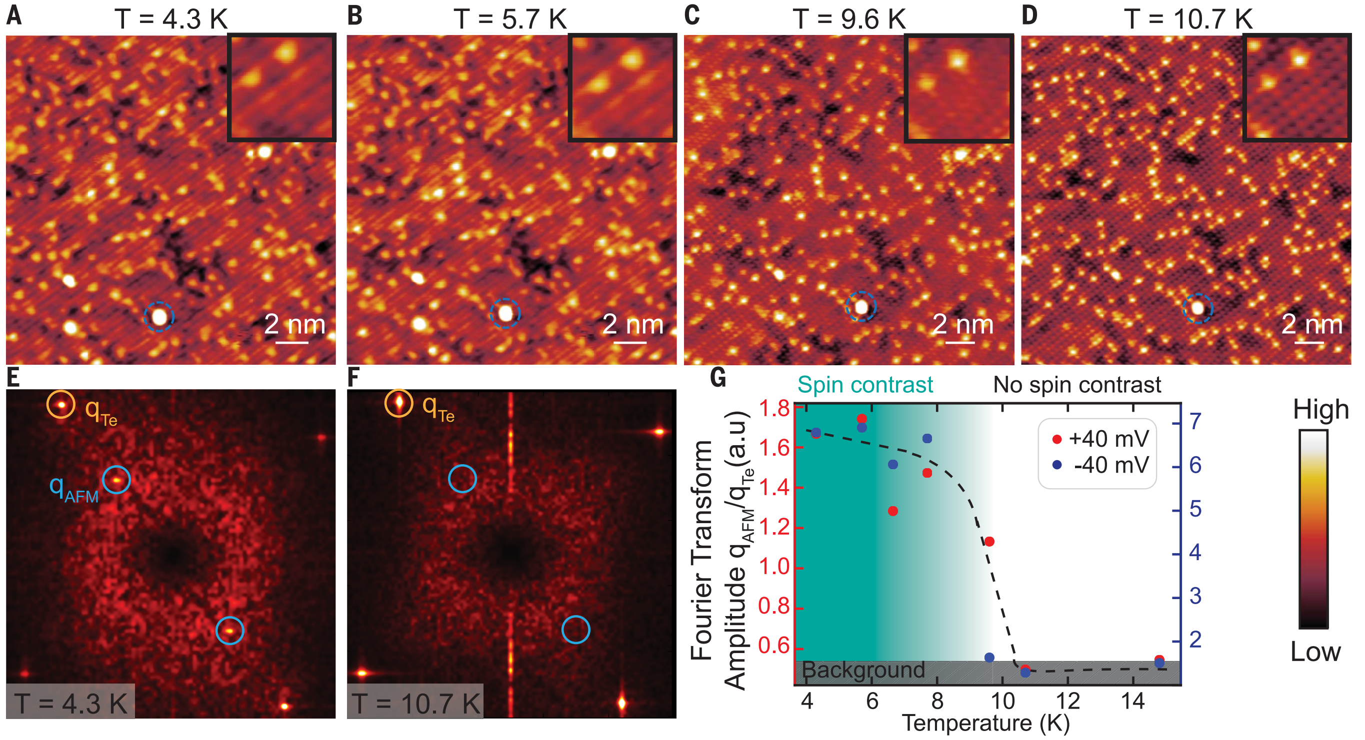

Fig. 3. Temperature dependence showing diminishing spin contrast. (**A** to **D**) STM topography on $Fe_{1+x}Te$ at the labeled temperatures obtained in the same field of view (V_{Bias} = 40 mV, I = 40 pA). Blue circles denote the same defect in all frames. (**E** and **F**) Comparison of FFTs of (A) and (D) to illustrate the disappearance of the q_{AFM} at 10.7 K, far below the antiferromagnetic T_C. A Gaussian background has been subtracted from the center to improve visualization of the q vectors. (**G**) Plot of the ratio of the intensity of the signal from q_{AFM} to the Bragg peak (q_{Te}) as a function of temperature. Black dashed line is a guide to the eye. The spin contrast signal from the AFM stripes is highly suppressed at ~10 K, similar to the behavior of the topological surface state.

using multiple nanowire tips (fig. S5) (*28*). Because it is well established that spin-dependent spatial contrast in STM images arises from the tunneling of spin-polarized electrons, the observed spin contrast directly indicates that the SmB_6 nanowire tips act as a source of spin-polarized currents.

As a first check of the possible involvement of the surface states in generating the spin-polarized currents, we measured the temperature dependence of the observed spin contrast. Previous transport and spectroscopic experiments on bulk SmB_6 have revealed the attenuation of the Dirac surface states in SmB_6 with increasing temperature and a transition from surface-dominated to bulk-dominated regime around 10 to 14 K (*15*, *16*, *34*, *35*). Figure 3, A to D, shows the temperature-dependent topographies of $Fe_{1+x}Te$ in the same field of view. The AFM order can be seen clearly at lower temperatures. However, at ~10 K, the striped signature of the AFM order disappears, leaving behind only the atomic corrugation of the Te lattice. This is also clearly seen in the fast Fourier transform (FFT) (Fig. 3, E and F). We obtained similar results with two other nanowire tips (fig. S6) (*28*). Upon cooling down, the AFM order reappeared (fig. S7) (*28*). Given that the Neel temperature (T_N) for $Fe_{1.03}Te$ is ~50 to 60 K, the disappearance of magnetic contrast around ~10 K must be caused by a change in the nanowire tip. In fact, previous STM images obtained with magnetic tips continued to show AFM order all the way to 45 K (*30*). In addition, we investigated the same samples with canonical spin-polarized Cr tips, which continued to show clear AFM stripes at 10 K (see fig. S8) (*28*).

Although the temperature dependence suggests a causal relationship between the presence of the surface states and the spin-polarized contrast (fig. S9) (*28*), there may be other explanations for the temperature dependence. For example, metallic Sm is AFM in nature and has a T_N of ~14 K (*36*), so a Sm cluster on the tip might create spin-polarized currents that mimic this temperature dependence. To distinguish between these scenarios, we explored how spin-momentum-locked tunneling of Dirac electrons is different from typical magnetic tips. We calculate the spin-resolved transport coefficients for tunneling between a normal two-dimensional (2D) metal and a 2D band of spin-momentum-locked, singly degenerate linearly dispersing states (Fig. 4D, schematic). A Zeeman term was used to open a gap in the inner band of 2D Rashba states, which mimics tunneling from a 2D Dirac band. The transmission coefficient with an infinitesimal bias voltage is equivalent to the differential conductance, and as is usual in tunneling, the sign of the bias voltage dictates the direction of travel of the tunnel current. The net spin polarization of the tunneling electrons going from left to right ($I_{L\text{-}R}$) and right to left ($I_{R\text{-}L}$) is plotted in fig. S10B (*28*). The calculations show two important features: (i) The tunnel current is indeed spin polarized and (ii) the spin polarization reverses when the direction of tunneling is reversed (helical tunneling). Such a reversal of spin polarization is neither expected nor observed for conventional magnetic tips (*37*), suggesting an unambiguous way to test the involvement of the surface states in generating spin-polarized currents by checking whether the currents are oppositely polarized at opposite bias.

From the discussion above, a "smoking gun" proof of the proposed helical tunneling would be the observation of contrast reversal of the observed AFM stripes at opposite tip bias voltages. Shown in Fig. 4, A and B, and in fig. S11 (*28*) are images in the same area obtained at positive and negative biases with a nanowire tip. The line cuts of the two images (Fig. 4C) show a reversal of the AFM contrast, indicating that the opposite spin channel is selected by the tunneling electrons upon switching the

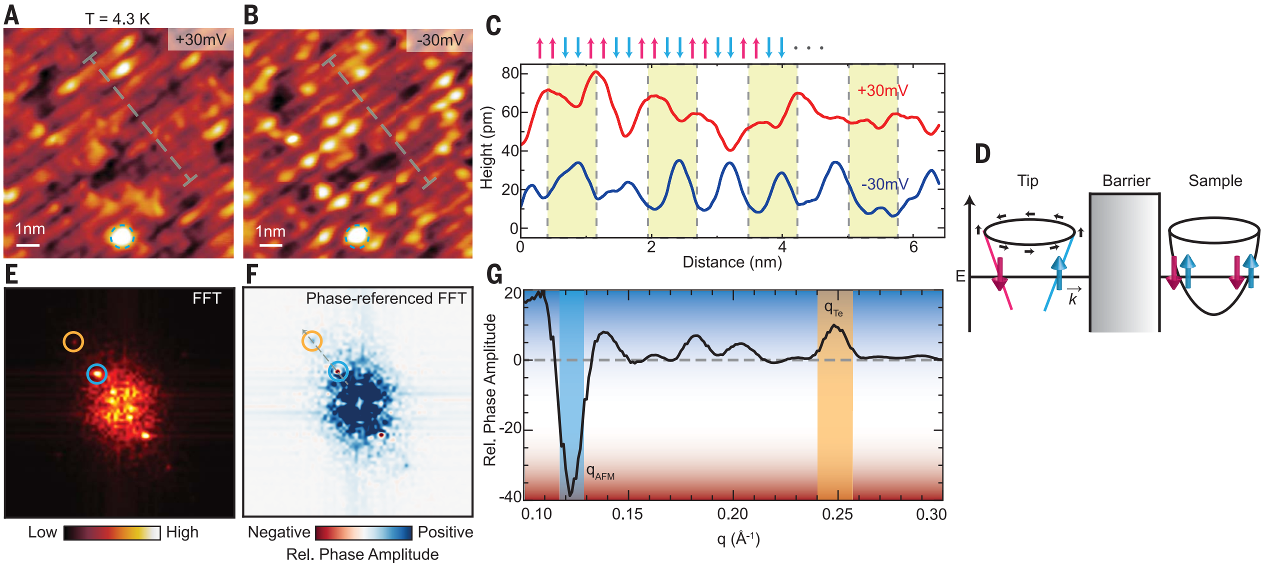

Fig. 4. Helical tunneling with a SmB$_6$ nanowire tip: Contrast reversal at opposite bias voltages. (**A** and **B**) STM topographies of Fe$_{1+x}$Te obtained in the same area at +30 mV (−30 mV) and using an SmB$_6$ tip at T = 4.3 K. (**C**) Height profile of the topography along gray dashed lines in (A) (red curve) and (B) (blue curve). The red curve is shifted vertically for clarity. The dotted lines correspond to the peaks of the red curve and dips of the blue curve, indicating a π-phase shift of the stripes between the positive and negative bias scan. (**D**) Illustration of the tunneling geometry used for the quantum tunneling simulation from the TSS to a normal metal. Without loss of generality, we have assumed the tip to be a 2D metal with just one branch of spin-momentum-locked states crossing the Fermi energy and the sample to be a normal metal with spin-degenerate bands (28). In reality, the sample has AFM stripes arising from the Fe lattice, which is visualized by the spin-polarized currents from the tip. (**E**) Absolute magnitude of the FFT of the topography shown in (B) showing the peaks associated with q_{Te} (yellow) and q_{AFM} (cyan). (**F**) Phase-referenced FFT between the topographies shown in (A) and (B), with the same peaks highlighted in cyan and yellow. The relative phase amplitude is negative at q_{AFM}, indicating a π-phase shift of the stripes originating from helical tunneling. (**G**) Line cut across the phase-referenced FFT [indicated by gray dashed line in (F)] illustrating the sign change between q_{Te} and q_{AFM}.

sign of the bias voltage. To better establish that this contrast reversal is pervasive over the whole image, we performed phase-referenced FFT (*38*) (see fig. S12 for the analysis method) (*28*). As shown in Fig. 4, F and G, we observed a negative value for the relative phase amplitude at the antiferromagnetic ordering vector (q_{AFM}), establishing a π-phase shift of the stripes at opposite biases. This contrast reversal was robust against thermal cycling (fig. S13) (*28*). Moreover, as expected, such contrast reversal was not observed for spin-polarized Cr tips [fig. S14 (*28*) and see (*38*)].

Combined with the temperature dependence, the contrast reversal at opposite bias voltages suggests that the topological surface states participate in generating the spin-polarized tunneling currents observed in our experiment. Although there are different facets on the nanowires, we expect the junction to be formed at the bottom of one of the side crystal planes (see schematic in fig. S15) (*28*). This is important because an equal average over all facets would lead to zero net spin polarization. Indeed, the macroscopic W wire, which hosts the nanowire, is slid into the tip holder and tightened by a set screw, which always causes a tilt, and this naturally results in the tunnel junction being formed at one of the side facets (see schematic in fig. S15) (*28*).

Further support for the involvement of the surface states was obtained by directly measuring how the low-energy features associated with the SmB$_6$ surface states change across the AFM stripes. Shown in Fig. 2I is a spectroscopic line cut across one period of the AFM stripe. We found that the amplitude of the low-energy features associated with the surface state changed periodically as the tip was moved across an AFM stripe. This change in intensity is a result of changes in the tunneling probability caused by the different relative orientations of the tip-surface state electron spin and the sample spin. This scenario of TSS-mediated helical tunneling will survive even with the weak surface magnetism that has been observed in SmB$_6$ at millikelvin temperatures (*24*). It has been suggested that the TSS may mediate a ferromagnetic RKKY interaction among magnetic impurities on the surface, giving rise to this surface magnetism (*39*). However, because the Dirac surface states are generated by the nontrivial topology of the bulk, weak surface magnetism would simply open a small (<1 meV) gap at the Dirac point, leaving the remainder of the helical tunneling physics outside of this energy window unchanged. This would not be at odds with any of our observations.

In summary, the reduced dimensionality and geometry of the nanowire tips allowed us to study the tunneling properties of a candidate TKI. Our observations and calculations show that the spin polarization of the tunnel current is insensitive to the position of the Fermi energy relative to the Dirac point and only depends on the direction of tunneling. These unique properties of spin-momentum-locked Dirac fermions may be used directly for manipulating spin currents in the field of spintronics. In addition, magnetic contrast at surfaces or local defects can be detected with atomic resolution without using external magnetic fields, as would be necessary in a traditional spin-polarized STM. Equally important, our technique of mounting nanowires on the STM tip opens up avenues for using topological nanowire tips for devices and heterostructures (*40*, *41*). As an example, a proximitized topological nanowire in a vertical magnetic field would host Majorana fermions at the end, effectively making a Majorana tip. This may then be used for directly studying interactions as a function of distance between two Majorana modes (one on the nanowire tip and the other on the sample), which has proven difficult to do so far. Finally, scanning probe microscopy using unconventional tips is a burgeoning field in the study of quantum materials for nanoscale magnetic imaging (*42*, *43*). Our work thus opens many avenues for using various kinds of functionalized nanowires as STM tips (superconducting, topological, etc.) for atomic-resolution imaging to provide nanoscale information on different materials properties such as magnetism, superconductivity, and other emergent excitations.

REFERENCES AND NOTES

1. M. Z. Hasan, C. L. Kane, *Rev. Mod. Phys.* **82**, 3045–3067 (2010).
2. K. L. Wang, M. Lang, X. Kou, "Spintronics of topological insulators," in *Handbook of Spintronics*, Y. Xu, D. Awschalom, J. Nitta, Eds. (Springer, 2016).
3. L. Šmejkal, Y. Mokrousov, B. Yan, A. H. MacDonald, *Nat. Phys.* **14**, 242–251 (2018).
4. Y. Tokura, K. Yasuda, A. Tsukazaki, *Nat. Rev. Phys.* **1**, 126–143 (2019).
5. C.-Z. Chang *et al.*, *Science* **340**, 167–170 (2013).
6. K. N. Okada *et al.*, *Nat. Commun.* **7**, 12245 (2016).
7. Y. Fan *et al.*, *Nat. Mater.* **13**, 699–704 (2014).
8. M. Dzero, K. Sun, V. Galitski, P. Coleman, *Phys. Rev. Lett.* **104**, 106408 (2010).
9. M. Dzero, J. Xia, V. Galitski, P. Coleman, *Annu. Rev. Condens. Matter Phys.* **7**, 249–280 (2016).
10. X. Zhang *et al.*, *Phys. Rev. X* **3**, 011011 (2013).
11. S. Rößler *et al.*, *Proc. Natl. Acad. Sci. U.S.A.* **111**, 4798–4802 (2014).
12. M. Neupane *et al.*, *Nat. Commun.* **4**, 2991 (2013).
13. W. Ruan *et al.*, *Phys. Rev. Lett.* **112**, 136401 (2014).
14. W. K. Park *et al.*, *Proc. Natl. Acad. Sci. U.S.A.* **113**, 6599–6604 (2016).
15. L. Jiao *et al.*, *Nat. Commun.* **7**, 13762 (2016).
16. H. Pirie *et al.*, *Nat. Phys.* **16**, 52–56 (2020).
17. V. Alexandrov, P. Coleman, O. Erten, *Phys. Rev. Lett.* **114**, 177202 (2015).
18. L. Li, K. Sun, C. Kurdak, J. W. Allen, *Nat. Rev. Phys.* **2**, 463–479 (2020).
19. S. Wolgast *et al.*, *Phys. Rev. B* **88**, 180405 (2013).
20. D. J. Kim *et al.*, *Sci. Rep.* **3**, 3150 (2013).
21. T. Liu *et al.*, *Phys. Rev. Lett.* **120**, 207206 (2018).
22. A. R. Mellnik *et al.*, *Nature* **511**, 449–451 (2014).
23. Q. Song *et al.*, *Nat. Commun.* **7**, 13485 (2016).
24. Y. Nakajima, P. Syers, X. Wang, R. Wang, J. Paglione, *Nat. Phys.* **12**, 213–217 (2016).
25. N. Xu *et al.*, *Nat. Commun.* **5**, 4566 (2014).
26. S. Lee *et al.*, *Nature* **570**, 344–348 (2019).
27. P. Hlawenka *et al.*, *Nat. Commun.* **9**, 517 (2018).
28. Materials and methods and supporting data are available as supplementary materials.
29. H. Gan *et al.*, *Cryst. Growth Des.* **19**, 845–853 (2019).
30. M. Enayat *et al.*, *Science* **345**, 653–656 (2014).
31. T. Hänke *et al.*, *Nat. Commun.* **8**, 13939 (2017).
32. S. Manna *et al.*, *Nat. Commun.* **8**, 14074 (2017).
33. R. Wiesendanger, *Phys. Rev. Lett.* **81**, 1495 (2009).
34. J. D. Denlinger *et al.*, Temperature dependence of linked gap and surface state evolution in the mixed valent topological insulator SmB$_6$. https://arxiv.org/abs/1312.6637 (2013).
35. F. Chen *et al.*, *Phys. Rev. B* **91**, 205133 (2015).
36. M. Mito *et al.*, *Phys. Rev. B* **104**, 054431 (2021).
37. M. Enayat, "Construction and operation of a milli-kelvin spectroscopic imaging STM for the study of correlated electron materials, PhD thesis, Swiss Federal Institute of Technology Lausanne (2014); https://www.fkf.mpg.de/5191581/dok92-Mostafa_Enayat_Thesis_2014.pdf.
38. S. Chi *et al.*, Determination of the superconducting order parameter from defect bound state quasiparticle interference. arXiv:1710.09089 [cond-mat.supr-con] (2017).
39. Q. Liu, C.-X. Liu, C. Xu, X.-L. Qi, S.-C. Zhang, *Phys. Rev. Lett.* **102**, 156603 (2009).
40. P. Liu, J. R. Williams, J. J. Cha, *Nat. Rev. Mater.* **4**, 479–496 (2019).
41. R. Lutchyn *et al.*, *Nat. Rev. Mater.* **3**, 52–68 (2018).
42. F. Casola, T. van der Sar, A. Yacoby, *Nat. Rev. Mater.* **3**, 17088 (2018).
43. D. Vasyukov *et al.*, *Nat. Nanotechnol.* **8**, 639–644 (2013).
44. Raw files and code for: A. Aishwarya *et al*,, Spin-selective tunneling from nanowires of the candidate topological Kondo insulator SmB6, Illinois Data Bank (2022); https://doi.org/10.13012/B2IDB-9971603_V1.

ACKNOWLEDGMENTS

We thank H. Zhou, Senior Research Scientist, Materials Research Laboratory, University of Illinois, for help in using the focused ion beam + SEM dual-beam system and S. Wirth and P. Xiong for helpful discussions. **Funding:** The STM work at the University of Illinois was supported by the National Science Foundation through grant DMR-2003784. M.H and T.L.H thank the Army Research Office (ARO) under Multidisciplinary University Research Initiatives (MURI) grant W911NF2020166 for support. V.M acknowledges partial support from the Gordon and Betty Moore Foundation (EPiQS grant 9465) and the Materials Research Laboratory Central Research Facilities at the University of Illinois for use of the cleanroom. V.M is a CIFAR Fellow in the Quantum Materials Program and acknowledges CIFAR for support. A.A. was partially funded by PPG-Materials Research Laboratory Graduate assistantship 2020-2021. X.L and F.L. are very thankful for the support of the National Science Foundation of China (grant 51872337) and the National Project for the Development of Key Scientific Apparatus of China (grant 2013YQ12034506). L.J. and X.W. acknowledges financial support from National MagLab, which is funded by the National Science Foundation (grant DMR-1644779) and the State of Florida. **Author contributions:** A.A., L.J., and V.M. conceived the experiments. A.A., A.R., and L.J. obtained the STM data and characterized the tips and samples. L. J., M.R., and Z.C. fabricated the nanowire tips. G.D.G. provided the single crystals of Fe$_{1.03}$Te. X.L. and F.L. grew the nanowires of SmB$_6$. X.W., M.H., and T.H. performed the theoretical modeling. A.A., L.J., and V.M. performed the data analysis and wrote the manuscript with help from all the authors. **Competing interests:** The authors declare no competing interests. **Data and materials availability:** All data have been uploaded to the Illinois Data Bank (*44*). **License information:** Copyright © 2022 the authors, some rights reserved; exclusive licensee American Association for the Advancement of Science. No claim to original US government works. https://www.science.org/about/science-licenses-journal-article-reuse

SUPPLEMENTARY MATERIALS

science.org/doi/10.1126/science.abj8765
Materials and Methods
Supplementary Text
Figs. S1 to S16
References (*45*–*47*)

Submitted 7 June 2021; resubmitted 8 January 2022
Accepted 5 August 2022
10.1126/science.abj8765